Correlation between Static and Dynamic Elastic Modulus of Soil by Triaxial Tests in Various Effective Consolidation Stresses

Van Hieu Nguyen
Le Quy Don Technical University, Hanoi, Vietnam
hieunv@lqdtu.edu.vn (corresponding author)

Van Thuy Do
Le Quy Don Technical University, Hanoi, Vietnam
thuydv@lqdtu.edu.vn (corresponding author)

Xuan Bang Nguyen
Le Quy Don Technical University, Hanoi, Vietnam
nxb@lqdtu.edu.vn

Duc Tiep Pham
Le Quy Don Technical University, Hanoi, Vietnam
phamductiep@lqdtu.edu.vn

Received: 5 February 2025 | Revised: 24 February 2025 | Accepted: 13 March 2025

 DOI: https://doi.org/10.48084/etasr.10466

ABSTRACT

This paper presents the behavior of gravelly soil specimens subjected to static and dynamic loading under undrained conditions, as investigated through laboratory triaxial tests. The experiments were performed on gravelly soil specimens with a relative compaction of 0.98 when the effective consolidation stress was varied with three different levels: 100 kPa, 150 kPa, and 180 kPa. The experimental results show that under the effect of static load and dynamic load in the undrained triaxial test, excess pore water pressure is formed during the loading process. After a period of applied load, the pore water pressure increases and causes specimen destruction. Then, the axial strain increases dramatically and is unable to recover. Regarding the change in effective consolidation stress on the specimen, the initial strength values increase as the effective consolidation stress increases. This is also expressed by the ratio of dynamic elastic modulus to the static one (E_d/E_0), which is equal to 1.587 in the effective consolidation stress of 100 kPa, 1.622 in the effective consolidation stress of 150 kPa, and 1.684 in the effective consolidation stress of 180 kPa. This study highlights the necessity to consider soil behavior under static and dynamic load to improve the understanding of soil mechanics and aid in the design of safer and more efficient structures.

Keywords-gravelly soil; static load; dynamic load; effective consolidation stress; triaxial tests

I. INTRODUCTION

Infrastructure stability is greatly affected by the mechanical behavior of subgrade soil under static and dynamic loading conditions. In order to ensure structural integrity and optimize foundation design, it is important to understand soil stiffness and how it responds to various stresses [1-3]. A great amount of research has examined the effect of settlement, deformation, and failure mechanisms, relying on soil engineering principles, such as stress-strain correlation, cohesion, and internal friction angles [4-7]. On the other hand, the behavior of soil under dynamic loading, including cyclic vehicular traffic and seismic forces, is more complex because it depends on factors, such as strain rate effects, stiffness degradation, and the potential of losing coherence and exhibiting fluid-like behavior. The elastic modulus is a critical parameter for quantifying soil stiffness, where static elastic modulus (E_0) is typically estimated through single loading tests, while dynamic elastic modulus (E_d) is calculated through cyclic or oscillating testing methods [8]. The correlation between E_0 and E_d is important for predicting soil behavior under varying loading conditions. A number of studies have attempted to determine the empirical correlations between E_0 and E_d for different soil types and loading conditions. Nevertheless, inconsistencies remain due to differences in experimental methods, soil composition, and

drainage conditions [9-12]. Furthermore, the influence of effective stress on the relationship between E_0 and E_d has not been extensively examined, especially for gravelly soils under undrained conditions. The current study tries to address this gap, evaluating the correlation between static and dynamic elastic modulus for gravelly soil specimens subjected to undrained conditions. A series of advanced triaxial tests were conducted under three distinct effective consolidation stress levels of 100 kPa, 150 kPa, and 180 kPa. By analyzing the relationship between E_0 and E_d across these stress levels, this study provides more understanding of the mechanical behavior of subgrade soils, allowing for more accurate predictions of soil stiffness under both static and dynamic loading conditions. The findings contribute to geotechnical engineering advancement by offering a refined empirical framework for assessing soil behavior, ultimately improving the reliability and efficiency of foundation and infrastructure designs.

II. RESEARCHED MATERIAL AND METHODS

A. Experimental Material and Specimen Reconstitution

The gravelly soil used for the subgrade (under the base layer) of Phan Thiet airport, in Binh Thuan Province, Vietnam, was obtained from the field and brought to the laboratory, as shown in Figure 1. The soil consists of gravel particles, small rocks, and various types of sticky soil particles. The soil's composition was analyzed through a grain-size curve presented in Figure 2, a relative compaction test shown in Figure 3, and a specific gravity test, with the examined parameters being presented in Table I.

Fig. 1. Gravelly soil for the experiment.

Authors in [10] determined the grain-size curve of gravelly soil, which is reformed to obtain a relative compaction (K) of 0.98, determined by [11-13]:

$$K = \frac{\gamma_k}{\gamma_k^{max}} \quad (1)$$

where K is the required relative compaction (dimensionless), γ_k is the dry density (T/m^3), and $\gamma_k^{\max}$ is the maximum dry density (T/m^3).

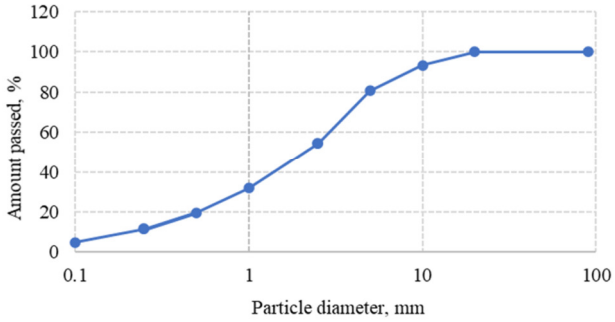

Fig. 2. Grain-size curve of the experimental soil.

The maximum dry density was determined by compacting the sample at five different moisture contents [14]. The maximum dry density is calculated as 2.112 T/m^3 with an optimum moisture content w_o of 7.59 %.

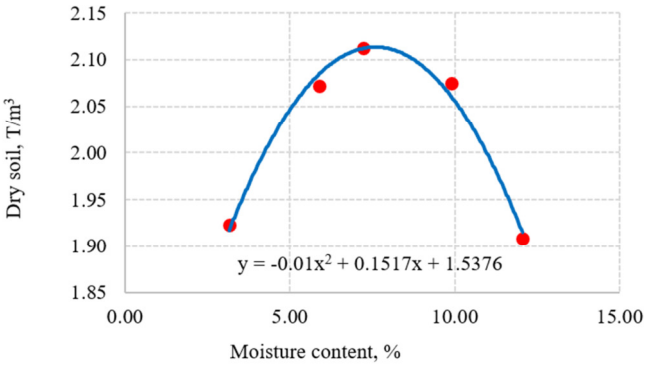

Fig. 3. Relationship curve of compacted dry soil and moisture content of soil.

TABLE I. TYPICAL PARAMETERS OF GRAVELLY SOIL

Characteristic	Symbol	Value	Unit	Applicable standards
Specific gravity	G_S	2.69	-	ASTM D7263-21
Effective grain size	D_{10}	0.221	mm	
Median grain size	D_{50}	2.220	mm	
Relative compaction	K	0.98	-	
Maximum dry unit weight	γ_k^{max}	2.112	T/m^3	ASTM D3080-11
Optimum moisture content	w_o	7.59	%	ASTM D3080-11

B. Methods

The triaxial test model is presented in Figure 4, and is based on ASTM standards [15-18].

1) Theoretical Methods of Soil Behavior Under Static and Dynamic Loads in Triaxial Tests

- Method of soil behavior under static load in triaxial tests

The first step is to allow the specimen to harden under conditions of constant isotropic stress and complete drainage (hardening phase). Subsequently, an axial load is applied, and water drainage is prevented (compression phase). During this phase, the change in pore water pressure is measured. From each set of recorded data, the relative axial strain can be calculated [19]:

$$\varepsilon_a = \frac{\Delta L}{L_c} \cdot 100 \quad (2)$$

where ε_a is the relative axial strain (%), L_c is the specimen length after consolidation (mm), ΔL is the portion of the length that changes from the original length during compression, determined by a strain transducer (mm).

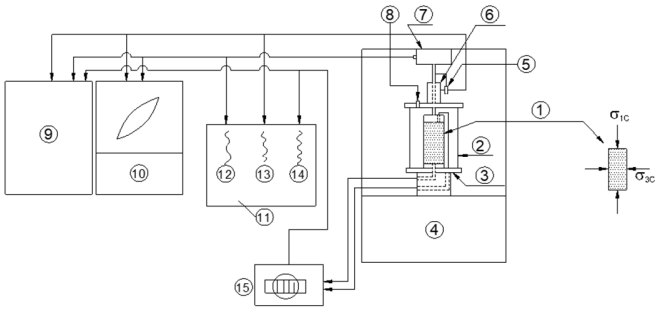

Fig. 4. Model of triaxial test (static and dynamic): (1) experimental specimen, (2) cell, (3) base, (4) triaxial compression frame creates static load, (5) vertical deflection transducer, (6) piston, (7) dynamic loading system, (8) confining pressure, (9) data acquisition, (10) x, y recorder, (11) strip chart, (12) loading chart, (13) vertical deformation chart, (14) volume change chart, (15) pore water pressure measurement device, σ_1 - major principal stress, σ_3 - minor principal stress.

It is hypothesized that the specimen deforms within a straight cylinder. Therefore, the cross-sectional area of the specimen is perpendicular to the axis A_s (mm²) as:

$$A_s = \frac{A_c}{1-\frac{\varepsilon_a}{100}} \quad (3)$$

where A_c is the initial area of the specimen perpendicular to its axis at the beginning of consolidation (mm^2). The axial force, P (N), presents an additional impact on the specimen that is independent of cell pressure:

$$P = (R - R_0) \cdot C_r \quad (4)$$

where R represents the readings on the force measuring device, R_0 is the initial reading of the force measuring device corresponding to the force acting on the specimen is zero, and C_r is the calibration factor of the force measuring device. The applied axial stress, i.e. the difference in principal stress, or measured deviator stress is calculated by:

$$(\sigma_1 - \sigma_3) = \frac{P}{A_s} \cdot 1000 \quad (5)$$

where $\sigma_1$is the major principal stress in a triaxial test (kPa) and σ_3 is the minor principal stress in a triaxial test (kPa). Considering the strength of the material specimen in the triaxial static compression test, the average modulus of elasticity E_{50} and the maximum static modulus of elasticity E_0 are parameters calculated from the graph of the relationship between the deviator stress and axial strain, as depicted in Figure 5.

In order to determine the cohesion c and the internal angle of friction φ of the soil, (6) can be used [17, 18]:

$$\varphi = arctg\left(\frac{A-1}{2\cdot\sqrt{A}}\right),\ c = \frac{\sigma_0}{2\cdot\sqrt{A}} \quad (6)$$

where $A = \frac{n\cdot\sum_{i=1}^{n}(\sigma_{1i}\cdot\sigma_{3i}) - \sum_{i=1}^{n}\sigma_{1i}\cdot\sum_{i=1}^{n}\sigma_{3i}}{n\cdot\sum_{i=1}^{n}(\sigma_{3i})^2 - \left(\sum_{i=1}^{n}\sigma_{3i}\right)^2}$,

$\sigma_0 = \frac{\sum_{i=1}^{n}\sigma_{1i}\cdot\sum_{i=1}^{n}(\sigma_{3i})^2 - \sum_{i=1}^{n}\sigma_{3i}\cdot\sum_{i=1}^{n}(\sigma_{1i}\cdot\sigma_{3i})}{n\cdot\sum_{i=1}^{n}(\sigma_{3i})^2 - \left(\sum_{i=1}^{n}\sigma_{3i}\right)^2}$ with $n = 3$, σ_{1i} is the major principal stress with effective consolidation stress in the ith experiment (kPa), σ_{3i} is the cell pressure with effective consolidation stress in the ith experiment (kPa), and n is the number of experiments.

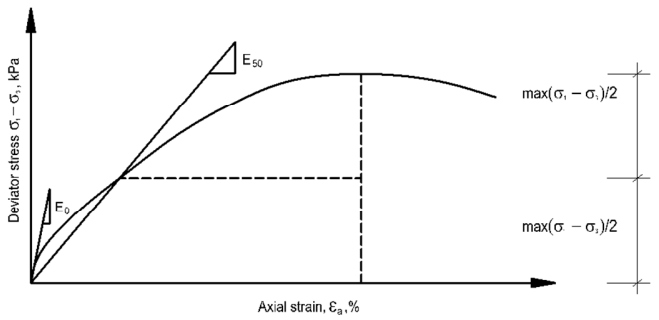

Fig. 5. Stress-strain relationship and determination of static elastic modulus of soil.

- Method of soil behavior under dynamic load (cyclic load in undrained condition) in triaxial tests:

The basic relationship of the dynamic parameters is determined by the axial stress and strain in the specimen [16]. The axial stress and strain in the specimen can be obtained from its response to increasing dynamic loading. The maximum dynamic shear stress τ_d and dynamic strain δ_d in the specimens are:

$$\tau_d = \frac{\sigma_d}{2} \quad (7)$$

$$\delta_d = (1 + \mu) \cdot \varepsilon_d \quad (8)$$

where σ_d is the maximum dynamic stress in the specimen (kPa), ε_d is the maximum dynamic strain in the specimen (mm), and μ is the Poisson's coefficient of the material. The dynamic modulus of elasticity (Young's modulus) is determined from the stress-strain behavior of the soil under cyclic axial loading, as demonstrated in [9], and can be calculated as:

$$E_d = \frac{\sigma_d}{\varepsilon_d} = \frac{\frac{(\sigma_{d1}-\sigma_{d2})}{2}}{\frac{(\varepsilon_{d1}-\varepsilon_{d2})}{2}} \quad (9)$$

where σ_{d1} is the maximum value of the axial compressive stress (kPa), σ_{d2} is the maximum value of the axial tensile stress (kPa), ε_{d1} is the maximum value of the axial compressive strain (mm), and $\varepsilon_{d1}$is the maximum value of the axial tensile strain (mm). Therefore, the dynamic shear modulus of a specimen is defined as:

$$G_d = \frac{E_d}{2\cdot(1+\mu)} \quad (10)$$

The damping ratio is a key dynamic parameter of the soil that expresses the hysteresis characteristic of its stress-strain behavior under cyclic loading, which is determined as [15]:

$$D = \frac{A_L}{4 \cdot \pi \cdot A_T} \cdot 100\% \quad (11)$$

where A_L is the area inside the hysteresis loop (kN·m), A_T is the area of the triangle (kN·m), calculated as: $A_T = 0.5 \cdot L \cdot S$, with L being the edges joined by the hysteresis loop (kN) and S the coordinate axes (m).

2) Experimental Method for Soil Specimens Subjected to Static and Dynamic Loads in Triaxial Tests

- Reconstituting specimen stage

The soil mass and water amount required to create moisture for the specimen must be determined according to the maximum dry density and optimum moisture content of the specimen at the relative compaction studied. The rubber membrane is then to be placed on the specimen mold, which is sealed at the bottom and top with rubber rings. The specimen should be subsequently compacted into the mold, resulting in a reconstituted specimen with a diameter of 7 cm and a height of 14 cm [13]. To ensure that the soil in the mold reaches the required relative compaction, it is divided into five equal parts and the compaction is measured by marking on the rammer. It is important that the specimens be thoroughly sealed to ensure the integrity of the experiment.

- Natural saturation stage

Prior to the removal of the prototyping mold, the specimen should be vacuumed. Subsequently, the triaxial cell should be positioned, and the vented water from the tank should enter the triaxial cell. The initial pressure has been created in the triaxial cell to stabilize the specimen when it is no longer under vacuum. The carbon dioxide is then aerated through the specimen by the Pore and Back systems for a duration of 30-40 min, with the objective of expelling all other gases within the specimen [13]. Following this, the specimen undergoes natural saturation by the circulation of degassed water through the specimen via the Pore and Back systems. The water diffuses the carbon dioxide within the specimen, subsequently filling the voids with water [13].

- Saturation stage by device

Start the air compressor, gauge, and computer, while increasing the cell pressure and back pressure values, until the saturation value B ≥ 0.95 (and is displayed on the computer). Record the back pressure value at the time of the saturation stop.

- Consolidation stage by device

Set the back pressure target to the value at the previous saturation stop. The cell pressure target value is equal to the back pressure value plus the effective consolidation stress. Merge the specimen until the degree of consolidation is greater than 98%, then stop.

- Stage of performing the load.

In the context of static load analysis, the following must be considered: The Dyna Triaxial software is used to set parameters, such as the compression loading method, ultimate strain, Tritech displacement control, and undrained condition [17]. Subsequently, the axial load will increase, and the water will not be permitted to drain (compression phase). It is important to note that the static loading is strain controlled. For the dynamic load, the parameters were set on Dyna Triaxial software, including the undrained condition, sinusoidal load, loading frequency, effective consolidation stress, loading amplitude, and the number of observation cycles [16, 19]. After that, the "Cyclic shear" mode should be selected, and the dynamic load should be initiated. In the dynamic loading experiment, the loading frequency was set to 0.25 Hz, and the loading amplitude was gradually increased from 10 kPa, to 20 kPa, 30 kPa, and 50 kPa, corresponding to 100 observation cycles with the first three levels of loading amplitude. The experiment continued until the specimen was damaged at a loading amplitude of 50 kPa. It is noteworthy that the steps involved in both static and dynamic loading tests are analogous in terms of specimen reconstitution, saturation, and consolidation. The present study examines the behavior of soil under static and dynamic loads, employing three distinct effective consolidation stresses (100 kPa, 150 kPa, and 180 kPa) on specimen models.

III. RESULTS AND DISCUSSION

A. Results

1) Soil Behavior Under Static Load

When static compression is applied with an effective consolidation stress of 100 kPa, the deflection stress, expressed by the axial deformation of the specimen, is shown in Figure 6. The experimental results and the graph exhibit that the soil specimen is completely deformed at the axial strain ε_a of 10.018%. At the moment of complete specimen damage, the deviator stress reaches a maximum value and then decreases. In the case of static compression with an effective consolidation stress of 150 kPa, the deviator stress, expressed through the axial deformation of the specimen, is presented in Figure 7.

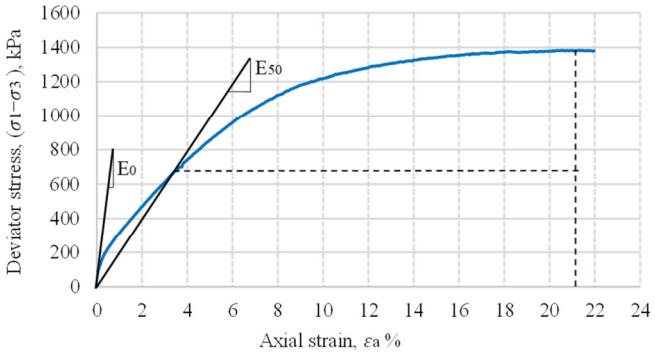

Fig. 6. Graph of relationship between deviator stress and axial strain of gravelly soil with effective consolidation stress of 100 kPa.

As illustrated in Figure 7, the experimental results and the graph indicate that the soil specimen undergoes complete deformation at an axial strain of 20.576%, known as the peak strain. At the moment of complete specimen damage, the deviator stress reaches a maximum value after which it begins to decrease. When static compression is applied with an

effective consolidation stress of 180 kPa, the deviator stress, expressed in terms of the axial deformation of the specimen, is portrayed in Figure 8. The experimental results and the graph indicate that the soil specimen undergoes complete deformation at an axial strain of 20.609%. At the moment of complete specimen damage, the deviator stress reaches a maximum value after which it decreases. In the static triaxial test for saturated, consolidated soil subjected to undrained compressive load, the behavior of soil specimens is also expressed through the excess pore water pressure formed during the loading process. The research findings concerning excess pore water pressure under the aforementioned three effective consolidation stresses are shown in Figure 9.

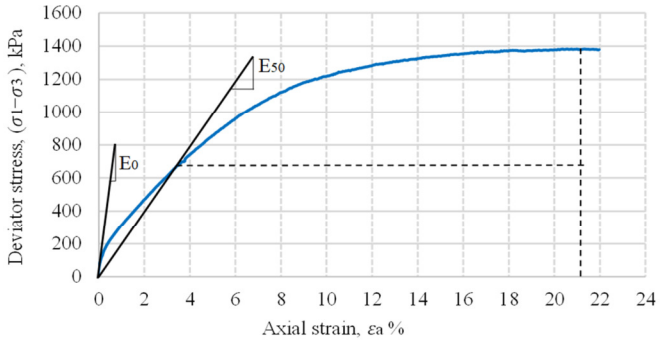

Fig. 7. Graph of relationship between deviator stress and axial strain of gravelly soil with effective consolidation stress of 150 kPa.

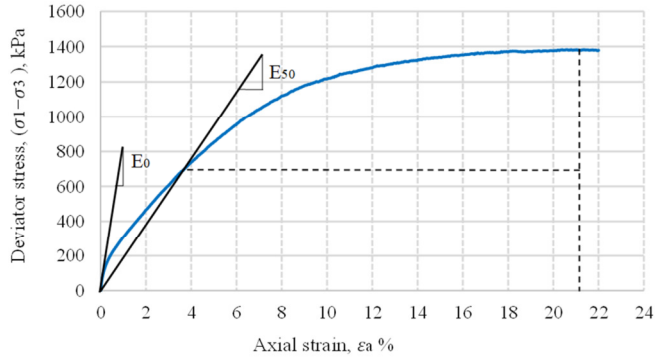

Fig. 8. Graph of relationship between deviator stress and axial strain of gravelly soil with effective consolidation stress of 180 kPa.

The initial excess pore water pressure exhibits a rapid increase, indicating compression of the pores in the specimen. Conversely, as the axial strain increases, leading to specimen destruction, the excess pore water pressure undergoes a substantial decline. For an effective consolidation stress of 100 kPa, the initial excess pore pressure of the specimen has a value greater than 40 kPa. This indicates that the load-bearing process of the specimen at a low consolidation stress level causes the specimen to fail quickly. This finding aligns with the outcomes of prior triaxial tests on sandy soils, where specimens with low confining pressures exhibited marginally higher initial excess pore pressures due to diminished stiffness and more moderate structural alterations during loading. These outcomes are consistent with the mechanical behavior of granular materials under different confining pressures [2, 7]. Table II presents the data considered to calculate the static elastic modulus of gravelly soil corresponding to three effective consolidation stresses, derived from the experimental results, while Table III presents the pressure and stress parameters, necessary to determine the cohesion and internal friction angle of gravelly soil, based on the experimental results.

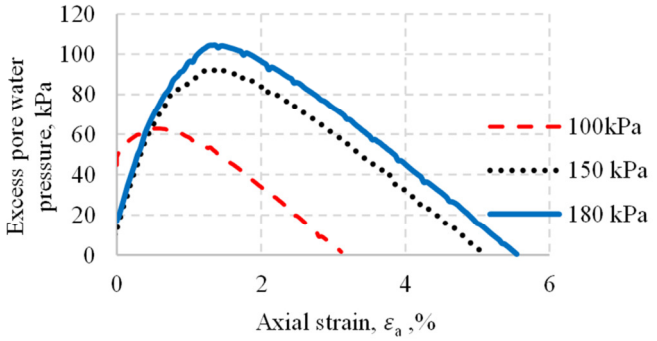

Fig. 9. Graph of change in excess pore water pressure according to axial strain of gravelly soil in various effective consolidation stresses.

TABLE II. STATIC ELASTIC MODULUS VALUES OF GRAVELLY SOIL AT THREE EFFECTIVE CONSOLIDATION STRESSES

Effective consolidation stress (kPa)	**Stress and strain to determine E_{50}**			**Stress and strain to determine E_0**		
	Deviator stress (kPa)	Axial strain (%)	E50 (MPa)	Deviator stress (kPa)	Axial strain (%)	E_0 (MPa)
100	605.890	3.259	18.591	55.746	0.070	79.637
150	700.508	3.765	18.606	116.985	0.118	99.055
180	711.686	3.789	18.781	88.459	0.084	104.913

TABLE III. PARAMETERS TO DETERMINE COHESION AND INTERNAL FRICTION ANGLE

Parameters	**Effective consolidation stress**		
	100 kPa	150 kPa	180 kPa
Deviator stress $\sigma_1 - \sigma_3$ (kPa)	1,211.78	1,383.21	1,383.70
Cell pressure σ_3 (kPa)	380	435	445
Major principal stress σ_1 (kPa)	1,591.78	1,818.21	1,828.70

According to (6): $c = 38.10$ kPa; $\varphi = 32.92^{\circ}$, the calculated cohesion and internal friction angle parameters indicate that the soil has relatively high cohesion due to the insertion of hooks and the bonding of discrete particles with each other at the studied density and moisture content. This is different from the soil in its natural state, where the particles are loose and not tightly bonded.

2) Soil Behavior under Dynamic Load

Applying cyclic loading in undrained condition with an effective consolidation stress of 100 kPa results in the strength and damping ratio data, as depicted in Figures 10 and 11, based on the axial strain of the specimen. The results indicate that as the axial strain increases, the dynamic Young's modulus decreases from 126.42 MPa, the shear modulus decreases from 42.14 MPa to almost no strength when the specimen is completely destroyed.

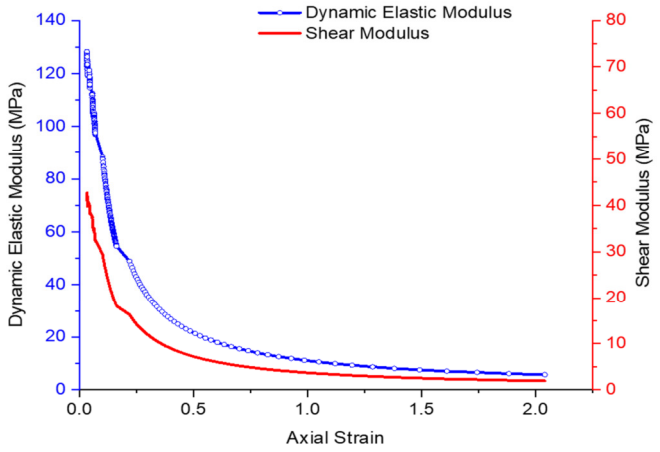

Fig. 10. Strength of gravelly soil specimen subjected to undrained cyclic loading with effective consolidation stress of 100 kPa.

Concurrently, the damping ratio exhibited an upward trend, ranging from 5.5% to a maximum of 12.98%, coinciding with the onset of specimen damage.

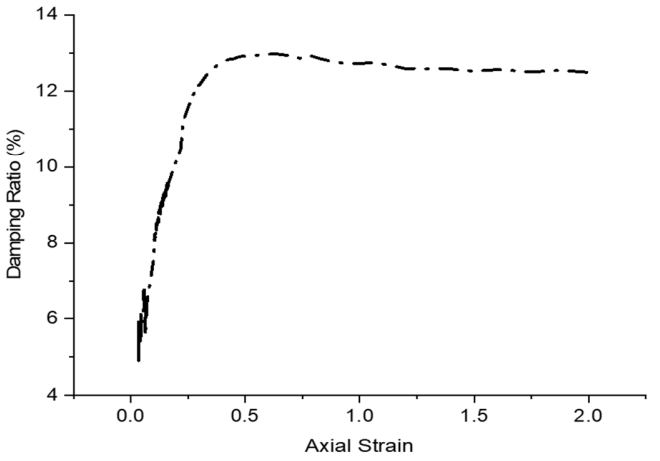

Fig. 11. Damping ratio of gravelly soil specimen subjected to undrained cyclic loading with effective consolidation stress of 100 kPa.

Applying cyclic loading in undrained condition, with an effective consolidation stress of 150 kPa, results in the acquisition of strength and damping ratio data, as presented in Figures 12 and 13, respectively, based on the axial strain of the specimen. The results show that as the axial strain increases, the dynamic Young's modulus decreases and the shear modulus decreases to almost zero when the specimen is completely destroyed. Meanwhile, the damping ratio tends to increase from 7.1% and reaches the maximum value of 13.57% when the specimen is damaged.

Applying cyclic loading in undrained condition with an effective consolidation stress of 180 kPa, results in the acquisition of strength and damping ratio data, as evidenced in Figures 14 and 15, respectively, based on the axial strain of the specimen.

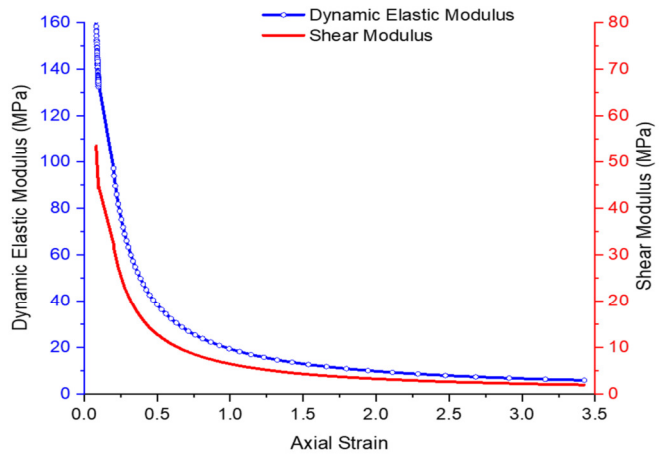

Fig. 12. Strength of gravelly soil specimen subjected to undrained cyclic loading with effective consolidation stress of 150 kPa.

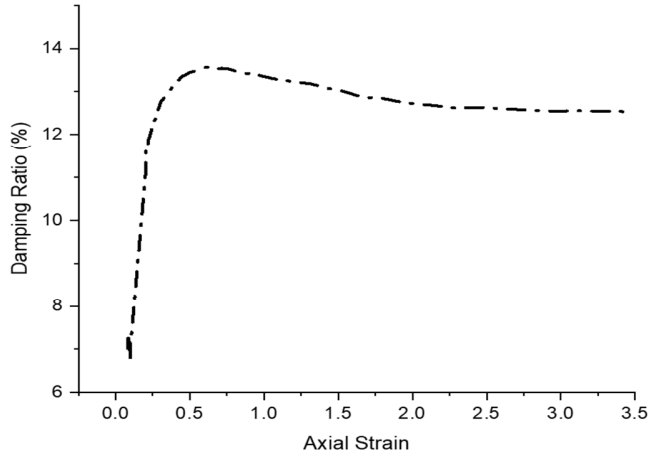

Fig. 13. Damping ratio of gravelly soil specimen subjected to undrained cyclic loading with effective consolidation stress of 150 kPa.

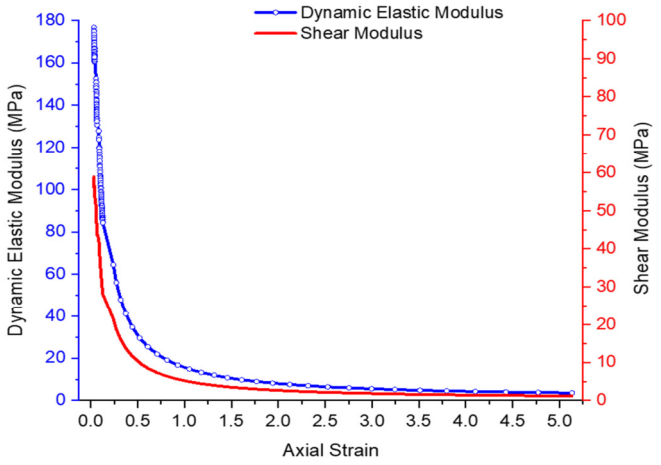

Fig. 14. Strength of gravelly soil specimen subjected to undrained cyclic loading with effective consolidation stress of 180 kPa.

The results revealed that as the axial strain increases, the dynamic modulus of elasticity decreases, the shear modulus

decreases to almost zero when the specimen is completely destroyed. Concurrently, the damping ratio exhibited an upward trend, ranging from 6.2% to a maximum of 15.42%, coinciding with the onset of specimen damage. Table IV presents the dynamic parameters of gravelly soil in the undrained cyclic load in various effective consolidation stresses, based on the experimental data.

3) Comparison of the Strength of Gravelly Soil Subjected to Static and Dynamic Loads

A comparative analysis of the dynamic elastic modulus and static elastic modulus of gravelly soil was conducted under varying effective consolidation stresses, as shown in Table V.

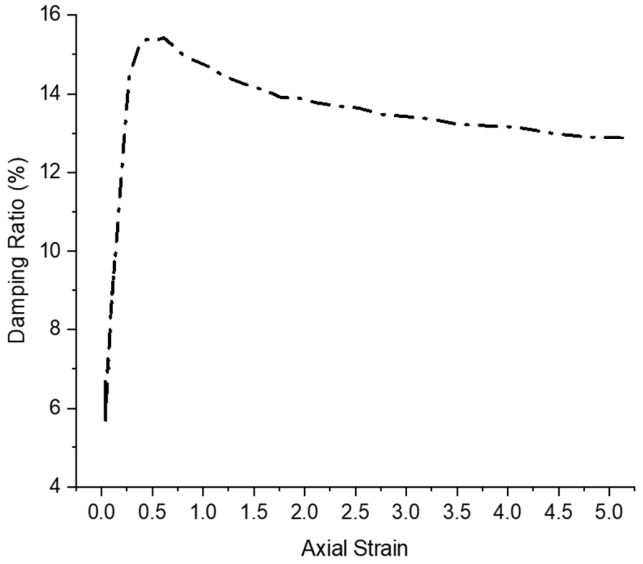

Fig. 15. Damping ratio of gravelly soil specimen subjected to undrained cyclic loading with effective consolidation stress of 180 kPa.

TABLE IV. DYNAMIC PARAMETERS OF GRAVELLY SOIL IN VARIOUS EFFECTIVE CONSOLIDATION STRESSES

Dynamic parameters	**Effective consolidation stress**		
	100 kPa	150 kPa	180 kPa
Dynamic elastic modulus (MPa)	126.42	160.69	176.64
Shear modulus (MPa)	42.14	53.56	58.88
Maximum damping ratio (%)	12.98%	13.57%	15.42%

TABLE V. ELASTIC MODULUS OF SOIL UNDER STATIC AND DYNAMIC LOADS

Parameters	**Effective consolidation stress**		
	100 kPa	150 kPa	180 kPa
Static elastic modulus E_0 (MPa)	79.637	99.055	104.913
Dynamic elastic modulus E_d (MPa)	126.42	160.69	176.64
$\frac{E_d}{E_0}$	1.587	1.622	1.684

B. Discussion

The results reveal that the soil behavior under static and dynamic loads changes significantly at different effective consolidation stresses, demonstrating its complexity. An increase in effective consolidation stress from 100 kPa to 180 kPa resulted in a modest rise in the elastic modulus E_{50}. This observation indicates that gravelly soil possesses a relatively stable stiffness, exhibiting good resistance to deformation, a property that may be related to the coarse grain structure that includes many types of grains in the composition. Additionally, the specimens appear to have a well-compacted structure with a relative compaction of 0.98 under the effective consolidation stresses studied. The initial excess pore water pressure exhibits a rapid increase due to the compression of the specimen's pores under axial compressive static load in undrained conditions. Subsequently, as the axial strain increases and the specimen is destroyed, the excess pore water pressure decreases significantly [15, 17, 18]. When examining the strength of a soil specimen based on the static modulus of elasticity, it is observed that it increases as the effective consolidation stress increases. In the context of deformability, when the effective consolidation stress is set at 100 kPa, the specimen undergoes complete damage at an axial strain of εa = 10.018%. In the other two cases, the specimen was destroyed at higher axial strain [4]. The calculated data indicate that the soil possesses a cohesion of 38.10 kPa and an internal friction angle of 32.92°, which is in line with the insertion of hooks and the bonding of discrete particles with the studied density and moisture content [20]. These parameters are critical in the field of soil mechanics research, as they provide a quantitative measure of the material's shear resistance and can be included into the analysis of construction foundations. The specimen's strength undergoes a decline in response to dynamic load, defined as a cyclic load in undrained conditions, resulting in an increase in axial strain. Moreover, the damping ratio gradually increases until the specimen is destroyed in complete deformation [15]. The axial strain of the specimen in all cases almost the same, with a value of approximately 0.6 at the time of specimen failure, representing the maximum damping ratio. In a similar manner to the applied static load, the strength of the specimen under dynamic loading also increases with an increasing effective compressive stress [21]. A notable finding is that the damping ratio values in this study are higher than the damping ratio of the river sand examined in [10]. This discrepancy can be attributed to the distinct material characteristics and particle compositions exhibited by these materials. A comparison of the static and dynamic elastic modulus of soil reveals that the dynamic one consistently exceeds the static one, particularly when considering maximum moment values. As the effective consolidation stress increases, the ratio between the dynamic and static elastic modulus rises gradually. This correlation is of theoretical and practical significance in calculation and design with different standards. The variation in effective consolidation stresses plays a critical role in the operation of diverse loads, contingent on the nature of the construction. For instance, in the context of foundation depth construction for traffic loads, soil strength undergoes changes in a saturated state, making it incapable of being dewatered under variable loads.

IV. CONCLUSIONS

The change of effective consolidation stress acting on the specimen significantly influences the strength of the building foundation under different loading conditions, especially when is flooded completely and drainage is difficult. In such

instances, the soil under load can cause serious damage to the foundation. This study underscores the significance of examining soil behavior under both static and dynamic loads, considering the range of effective consolidation stresses, to enhance engineers' understanding of how the soil responds to different loading conditions. This is essential for ensuring the stability and safety of structures, such as buildings, bridges, dams, roads, airports, etc. The undrained state is a condition in which the soil is unable to support the load, while the excess pore water pressure generated during loading is not reduced and can significantly affect soil behavior. The undrained response of soil specimens may involve phenomena, such as pore pressure build-up, contraction or dilation behavior, and destructive potential under certain loading conditions. The results demonstrate that the effective consolidation stress greatly influences the soil behavior and the strain generated under both static and dynamic loading. It is evident that an increase in effective consolidation stress results in higher strength under both loading conditions. The initial excess pore water pressure increases rapidly under the effect of a static load due to the compression of the specimen's pores. Subsequently, as axial strain increases, the specimen exhibits a tendency to break and the excess pore water pressure decreases significantly. The gravelly soil in this study exhibits a relatively stable stiffness and good resistance to deformation. This is possibly due to its coarse grain structure, which includes a wide variety of grains in its composition. The specimens appear to have a well-compacted structure, and the elastic modulus E_{50} increases, but not significantly, when the effective consolidation stress is increased. The specimen undergoes a rapid deformation under the effect of dynamic load, with a sudden and irreversible increase in axial strain at the time of failure. Additionally, a considerable increase in pore water pressure is a factor that may cause specimen damage. As the axial strain increases, the specimen's strength decreases, while its damping ratio gradually increases. It is noteworthy that until a complete deformation of the destroyed specimen occurs, the strength is almost absent and the damping ratio reaches the maximum value. The experimental findings demonstrate that the dynamic elastic modulus consistently exceeds the static one, particularly when considering maximum moment values, as evidenced by the ratio E_d = (1.587 - 1.684)·E_0. The correlation between soil strengths under static and dynamic loads is critical in applying parameters in design and calculations based on different standards when one of the two values is known. This finding provides a basis for engineers to combine with simulation software in order to understand the behavior of soil under the effects of static and dynamic loads.

REFERENCES

[1] D. C. Ferreira and F. Massad, "Evaluation of stress history and undrained shear strength of three marine clays using semi-empirical methods based on Piezocone Test," *Soils and Rocks*, vol. 45, Mar. 2022, Art. no. e2022075221, https://doi.org/10.28927/SR.2022.075221.

[2] Z. Zhu *et al.*, "Effect of the loading frequency on the sand liquefaction behaviour in cyclic triaxial tests," *Soil Dynamics and Earthquake Engineering*, vol. 147, Aug. 2021, Art. no. 106779, https://doi.org/10.1016/j.soildyn.2021.106779.

[3] N. A. Tuan and P. Q. Chieu, "The Effect of Moisture and Fine Grain Content on the Resilient Modulus of Sandy Clay Embankment Roadbed," *Engineering, Technology & Applied Science Research*, vol. 11, no. 3, pp. 7118–7124, Jun. 2021, https://doi.org/10.48084/etasr.4152.

[4] J. T. H. Wu, C.-Y. Tung, M. T. Adams, and J. E. Nicks, "Analysis of Stress-Deformation Behavior of Soil-Geosynthetic Composites in Plane Strain Condition," *Transportation Infrastructure Geotechnology*, vol. 5, no. 3, pp. 210–230, Sep. 2018, https://doi.org/10.1007/s40515-018-0057-y.

[5] G. E. Barnes, *Soil Mechanics*. London, UK: Macmillan Education, 1995.

[6] J. C. Wang, M. J. Zhao, W. Chen, and K. Wang, "Comparison of Dynamic and Static Triaxial Test on the Soil-Rock Mediums," *Advanced Materials Research*, vol. 446–449, pp. 1563–1567, 2012, https://doi.org/10.4028/www.scientific.net/AMR.446-449.1563.

[7] J. Li, J. Cui, Y. Shan, Y. Li, and B. Ju, "Dynamic Shear Modulus and Damping Ratio of Sand–Rubber Mixtures under Large Strain Range," *Materials*, vol. 13, no. 18, Jan. 2020, Art. no. 4017, https://doi.org/10.3390/ma13184017.

[8] V. T. Phan and T. T. H. Nguyen, "Elastic and Deformation Characteristics of MSWI Bottom Ash for Road Construction," *Engineering, Technology & Applied Science Research*, vol. 10, no. 6, pp. 6389–6392, Dec. 2020, https://doi.org/10.48084/etasr.3817.

[9] T. Pham, Md. W. Zaman, and T. Vu, "Modeling Triaxial Testing with Flexible Membrane to Investigate Effects of Particle Size on Strength and Strain Properties of Cohesionless Soil," *Transportation Infrastructure Geotechnology*, vol. 9, no. 4, pp. 417–441, Aug. 2022, https://doi.org/10.1007/s40515-021-00167-6.

[10] *D422 - 63 Standard Test Method for Particle-Size Analysis of Soils*. West Conshohocken, PA, USA: ASTM International, 2002

[11] *D698-12 Standard Test Methods for Laboratory Compaction Characteristics of Soil Using Standard Effort*. West Conshohocken, PA, USA: ASTM International, 2021.

[12] B. M. Das and K. Sobhan, *Principles of Geotechnical Engineering*, 8th edition. Stamford, CT: Cengage Learning, 2013.

[13] T. D. Van, H. N. Van, and T. P. Duc, "Behavior of Sand Specimens Subjected to Cyclic Loads under Drained and Undrained Conditions in Variable Loading Amplitudes," *Jordan Journal of Civil Engineering*, vol. 18, no. 2, pp. 268–279, Mar. 2024.

[14] *D1557-12 Standard Test Methods for Laboratory Compaction Characteristics of Soil Using Modified Effort*. West Conshohocken, PA, USA: ASTM International, 2021.

[15] *D2850-23 Standard Test Method for Unconsolidated-Undrained Triaxial Compression Test on Cohesive Soils*. West Conshohocken, PA, USA: ASTM International, 2023.

[16] *D3999 Standard Test Methods for the Determination of the Modulus and Damping Properties of Soils Using the Cyclic Triaxial Apparatus*. West Conshohocken, PA, USA: ASTM International, 2019.

[17] *D4767-11 Standard Test Method for Consolidated Undrained Triaxial Compression Test for Cohesive Soils*. West Conshohocken, PA, USA: ASTM International, 2020.

[18] *D7181 - 20 Standard Test Method for Consolidated Drained Triaxial Compression Test for Soils*. West Conshohocken, PA, USA: ASTM International, 2020.

[19] I. J. Alhani, W. M. Albadri, M. J. M. Noor, S. Y. Wong, and K. Y. Wong, "Technique to Avoid Membrane Punching During Triaxial Test of Crushed Aggregate," *Transportation Infrastructure Geotechnology*, vol. 8, no. 3, pp. 349–360, Sep. 2021, https://doi.org/10.1007/s40515-020-00141-8.

[20] Geotech data, "Cohesion", https://www.geotechdata.info/parameter/cohesion.

[21] V. Jagodnik and Ž. Arbanas, "Cyclic Behaviour of Uniform Sand in Drained and Undrained Conditions at Low Confining Stress in Small-Scale Landslide Model," *Sustainability*, vol. 14, no. 19, Jan. 2022, Art. no. 12797, https://doi.org/10.3390/su141912797.